

pubs.acs.org/acssensors Article

## CRISPR-Cas12a Biosensor Array for Ultrasensitive Detection of Unamplified DNA with Single-Nucleotide Polymorphic Discrimination

Zhengyan Weng,<sup>†</sup> Zheng You,<sup>†</sup> Huijie Li,<sup>†</sup> Guangfu Wu, Yang Song, He Sun, Ava Fradlin, Camille Neal-Harris, Mengshi Lin, Xue Gao,\* and Yi Zhang\*



Cite This: ACS Sens. 2023, 8, 1489-1499



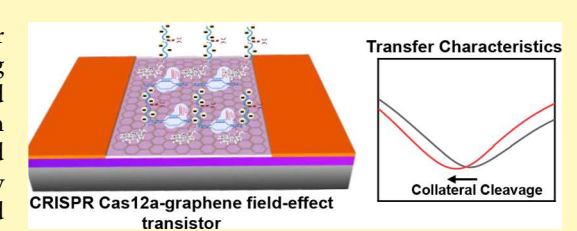
ACCESS I

III Metrics & More

Article Recommendations

Supporting Information

ABSTRACT: Quantitative polymerase chain reaction as a powerful tool for DNA detection has been pivotal to a vast range of applications, including disease screening, food safety assessment, environmental monitoring, and many others. However, the essential target amplification step in combination with fluorescence readout poses a significant challenge to rapid and streamlined analysis. The discovery and engineering of the clustered regularly interspaced short palindromic repeats (CRISPR) and CRISPR-associated (Cas) technology have recently paved the way for a novel approach to nucleic



acid detection, but the majority of current CRISPR-mediated DNA detection platforms are limited by insufficient sensitivity and still require target preamplification. Herein, we report a CRISPR-Cas12a-mediated graphene field-effect transistor (gFET) array, named CRISPR Cas12a-gFET, for amplification-free, ultrasensitive, and reliable detection of both single-stranded DNA (ssDNA) and double-stranded DNA (dsDNA) targets. CRISPR Cas12a-gFET leverages the multiturnover trans-cleavage activity of CRISPR Cas12a for intrinsic signal amplification and ultrasensitivity of gFET. As demonstrated, CRISPR Cas12a-gFET achieves a limit of detection of 1 aM for the ssDNA human papillomavirus 16 synthetic target and 10 aM for the dsDNA Escherichia coli plasmid target without target preamplification. In addition, an array of 48 sensors on a single 1.5 cm × 1.5 cm chip is employed to improve data reliability. Finally, Cas12a-gFET demonstrates the capability to discriminate single-nucleotide polymorphisms. Together, the CRISPR Cas12a-gFET biosensor array provides a detection tool for amplification-free, ultrasensitive, reliable, and highly specific DNA detections.

**KEYWORDS:** CRISPR-Cas12a, graphene field-effect transistor, amplification-free detection, ssDNA and dsDNA, single-nucleotide polymorphism

Recent technological advances in DNA testing have emerged into diverse aspects of biological applications, ranging from disease diagnosis, <sup>1-4</sup> prognosis, <sup>4,5</sup> and therapeutics, <sup>6,7</sup> to food safety inspection, <sup>8</sup> environmental monitoring, <sup>9,10</sup> biodiversity conservation, 11 security surveillance, 12 and forensic analysis.<sup>13</sup> To date, DNA detection has been predominantly relying on the identification of specific DNA sequences offered by nucleic acid amplification (NAA) such as nonisothermal polymerase chain reaction (PCR) and isothermal recombinase polymerase amplification (RPA). These conventional methods, despite being highly sensitive and specific, are generally confined to laboratory settings since they require expensive analytical instruments and a high level of expertise for sample treatment and assay preparation. 14,15 Consequently, NAAbased DNA testing often suffers from long turnaround time from sample collection to delivery of results, involving the transport of samples to licensed testing facilities and complicated, time-consuming processes of DNA extraction and amplification.<sup>14</sup> Although ongoing efforts have largely simplified and sped up the entire detection procedure, for example, by employing extraction-free strategies, 16-19 developing an integrated sample-to-result platform, <sup>19–22</sup> or introducing sample pooling, <sup>23</sup> these attempts have failed to completely address the critical challenges associated with NAA. More importantly, NAA is a nonlinear process with relative quantification against standard curves, <sup>22,24</sup> suggesting that the reliability of results is heavily dependent on a variety of factors, such as template quality, primer efficiency, impurities in matrices, and operating procedures. <sup>22,24–26</sup> Altogether, it is highly desirable to develop alternative amplification-free nucleic acid detection platforms to circumvent these issues.

Current amplification-free technologies for DNA detection primarily exploit base pair complementarity for highly specific sequence recognition; however, most techniques do not

Received: November 14, 2022 Accepted: March 14, 2023 Published: April 7, 2023





possess sufficiently high sensitivity, especially in clinical diagnostics where a minimum of femtomolar sensitivity is desired.<sup>27</sup> Derived from the prokaryotic adaptive immune system,<sup>28</sup> the clustered regularly interspaced short palindromic repeats (CRISPR)/CRISPR-associated (Cas) technology has paved a novel path for ultrasensitive DNA detection without target amplification.<sup>29</sup> As one of the first identified CRISPR-Cas systems, Cas9 exhibits double-stranded DNA (dsDNA) targeting capability when complexing with a guide RNA sequence.<sup>30</sup> CRISPR-Chip took advantage of the binding affinity of the catalytically inactive Cas9 complex to the target sequence and demonstrated amplification-free detection of Duchenne muscular dystrophy-associated mutations on a graphene field-effect transistor (gFET) with a limit of detection (LOD) of 1.7 fM.<sup>31</sup> This platform was later validated to discriminate single-nucleotide polymorphisms (SNPs) with a similar femtomolar sensitivity.<sup>32</sup> Nevertheless, the on-target recognition of dsDNA by Cas9 limits its ability to become a universal tool for DNA detection. Type II-C Cas9 variants can target single-stranded DNAs (ssDNAs), but they have limited dsDNA binding activity.<sup>33</sup> Moreover, using different Cas9 orthologs requires further optimization of the detection assay and introduces additional complexity. The discovery of CRISPR-Cas12 that can detect both ssDNA and dsDNA offers a promising solution. Remarkably, the Cas12 system can perform nonspecific cleavage of bystander ssDNA probes, known as collateral or trans-cleavage activity, upon the detection of target DNA sequences.<sup>34</sup> Such collateral activity converts a single target recognition event into multiple turnovers of probe cleavage and therefore, provides intrinsic signal amplification compared with conventional single-turn-over Cas9-mediated detection. So far, CRISPR-Cas12 systems have been integrated with diverse readout methods for amplification-free DNA detection, including fluorescence,<sup>37–</sup> electrochemiluminescence, 40 surface-enhanced Raman spectroscopy, 41 electrochemical sensing, 42 and nanopore sensing, 43 Yet, the detection limit of most of these methods lies within the femtomolar-to-picomolar range. As a result, there has been increasing interest in more sensitive amplification-free CRISPR-based DNA detection platforms.

We have previously developed a set of CRISPR-based RNA detection platforms without the need for target preamplification by (1) coupling CRISPR Cas13a with ultrasensitive detection platforms of gFETs<sup>44</sup> or (2) engineering Cas13a proteins for enhanced collateral activities.<sup>45</sup> Nevertheless, these platforms are limited to detecting RNA samples only; a lengthy and complicated reverse transcription step is needed to detect DNA targets. Additionally, the relatively large device-to-device variations challenge the detection reliability. Finally, there has been no demonstration of whether these platforms are able to distinguish SNPs, which constitute nearly 60% of known disease-associated variations in human genes.

Herein, we report a new class of CRISPR-based biosensor, named Cas12a-gFET, to accommodate the ever-growing need for DNA detection. This platform exploits the Cas12a-mediated multiturnover collateral cleavage of nonspecific DNA probes for signal amplification and transduces the signals via ultrasensitive gFET. The high carrier mobility of graphene allows gFET to sensitively probe biorecognition events occurring at the surface. Consequently, the synergistic effect of Cas12a signal amplification and gFET transduction enables the ultrasensitive readout of amplified outputs from collateral cleavage of probes anchored on the graphene surface, which

affords the attomolar sensitivity of CRISPR Cas12a-gFET, beyond the femtomolar level of Cas9-based gFET biosensor CRISPR-Chip<sup>31</sup> and SNP-Chip.<sup>32</sup> Moreover, we adopt a 48channel array design on a single sensor chip for enhanced reliability by reducing the effects of measurement outliers as a result of device-to-device variations. Compared with CRISPRbased optical methods, like CRISPR-Cas12a-mediated SERS assay, 46,47 CRISPR Cas12a-gFET eliminates the need for expensive optical labels and modules and therefore is more compatible with point-of-use applications (Table S1). The versatility for ultrasensitive identification of various DNA sequences is demonstrated by the detection of both bacterial DNA target from Escherichia coli with an LOD of 10 aM and DNA virus human papillomavirus 16 (HPV-16) with an LOD of 1 aM. Finally, our device successfully discriminates SNPs beyond simple differentiation of different pathogen targets. Together, CRISPR Cas12a-gFET array offers a promising solution to ultrasensitive, reliable, and highly specific DNA detection free of target amplification.

## RESULTS

Working Principle of CRISPR Cas12a-gFET for DNA Detection. The ultrasensitive CRISPR Cas12a-mediated amplification-free DNA detection leverages the synergy of multiturnover Cas12a collateral activities for intrinsic signal amplification and high-performance sensing capabilities of gFET enabled by the exceptional carrier mobility of graphene for sensitive probing of changes in the local electric field. Cas12a recognizes the hairpin structure of crRNA and forms a functional ribonucleoprotein (RNP) complex that can bind to the DNA target via base pairing between crRNA spacer and target sequence, 48,49 thereby resulting in high specificity of the system. The binding of ssDNA or dsDNA target initiates target-specific cis-cleavage as well as trans-cleavage of bystander ssDNA probes in a sequence-independent manner,<sup>34</sup> and this trans-cleavage process demonstrates a multi-turnover behavior over target binding,<sup>34</sup> suggesting a promising biological transduction pathway for amplified signal generation.

Here, we combine this mechanism with the unique working principle of field-effect transistor (FET) for ultrasensitive DNA detection. A typical three-terminal FET device has a pair of source-drain electrodes connected by a FET channel for current flow, and the third electrode, called gate electrode, provides an external electric field to regulate the charge carrier density in the FET channel, thereby modulating the channel conductivity and ultimately the source-drain current. This modulation, known as the field effect, is characterized by transfer characteristics that define the relationship between the source-drain current and the gate voltage at a constant source-drain voltage.<sup>50</sup> For biosensing applications, local biorecognition events at the surface of the FET channel alter the charge carrier density and are transduced into a shift in transfer characteristics.<sup>51</sup> Among a variety of FET channel materials, graphene, a two-dimensional (2D) nanomaterial made of a monolayer of sp<sup>2</sup> hybridized carbon atoms in a honeycomb lattice, <sup>52,53</sup> is an excellent candidate for its high mechanical strength, <sup>54</sup> specific surface area, <sup>53</sup> thermal conductivity, <sup>55</sup> and charge carrier mobility. <sup>52</sup> The zero bandgap of graphene leads to the free movement of charge carriers and contributes to the exceptional electrical conductivity. The ambipolarity of graphene indicates that under an external electric field, the charge carriers can be tuned between negatively charged electrons and positively-charged holes. 52

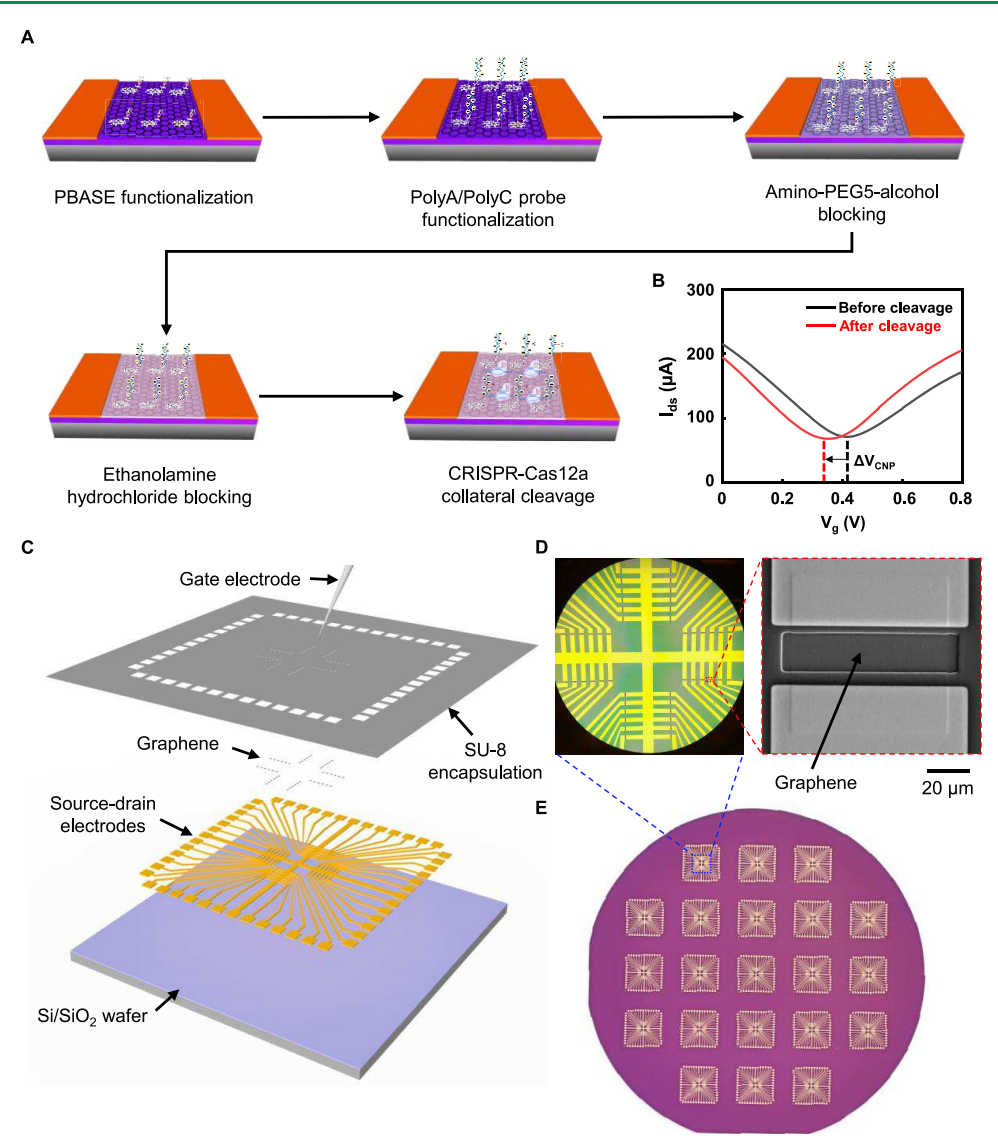


Figure 1. CRISPR Cas12a-gFET biosensor array for ultrasensitive and reliable detection of unamplified DNA. (A) Step-by-step illustration of DNA detection using CRISPR Cas12a-gFETs. (B) Demonstration of charge neutrality point (CNP) voltage  $(V_{\rm CNP})$  shift for detection of the 1 nM *E. coli* plasmid target. (C) Exploded schematic of the 48-channel array. (D) Photograph of source-drain contact pads of gFETs (left) and a representative scanning electron microscope (SEM) image of a single gFET. (E) Optical image of a total of 21 devices fabricated on a 4-inch wafer; each device contains a 48-channel gFET array.

Consequently, gFET exhibits V-shaped transfer characteristics, in which the local minimum is referred to as the charge neutrality point (CNP). The shift in the gate voltage at CNP is used to determine the shift of transfer characteristics and thus quantify the number of biorecognition events. <sup>50</sup>

In the case of the CRISPR Cas12a-gFET biosensor (Figure 1A), negatively charged ssDNA probes tethered to the graphene surface via 1-pyrenebutyric acid N-hydroxysuccinimide ester (PBASE) linker are cleaved by Cas12a in the presence of target DNA, primarily causing a decrease in the gating effect. As a result, an increase in the electron carrier density is observed, leading to a left shift of transfer characteristics and CNP voltage (Figure 1B). In general, the collateral cleavage of Cas12a follows Michaelis—Menten kinetics; 34,56 therefore, probe cleavage in terms of the magnitude of the shift can be associated with the concentration of activated enzymes. When Cas12a is in excess over DNA targets, this concentration corresponds to the target concentration for quantitative measurement. To compensate for

device-to-device variations, the shift is standardized using the relative change in the charge neutrality voltage before  $(V_{\rm CNP,0})$  and after  $(V_{\rm CNP,1})$  CRISPR assay application (eq 1).

$$\Delta V_{\rm CNP} = \frac{V_{\rm CNP,1} - V_{\rm CNP,0}}{V_{\rm CNP,0}} \times 100\% \tag{1}$$

**Design and Fabrication of 48-Channel Biosensor Array.** Despite the outstanding properties of graphene, it is challenging to prepare 2D graphene sheets with identical parameters. Moreover, the transfer of chemical vapor deposition-grown graphene onto a desired substrate may lead to defects and/or impurities, causing device failure (defects) or significantly altering the properties of graphene via doping (impurities). In addition, parasitic effects such as contact resistance between the graphene channel and the source—drain electrodes may also introduce additional artifacts. These issues suggest relatively large device-to-device variations among gFETs compared with conventional biosensor platforms. One

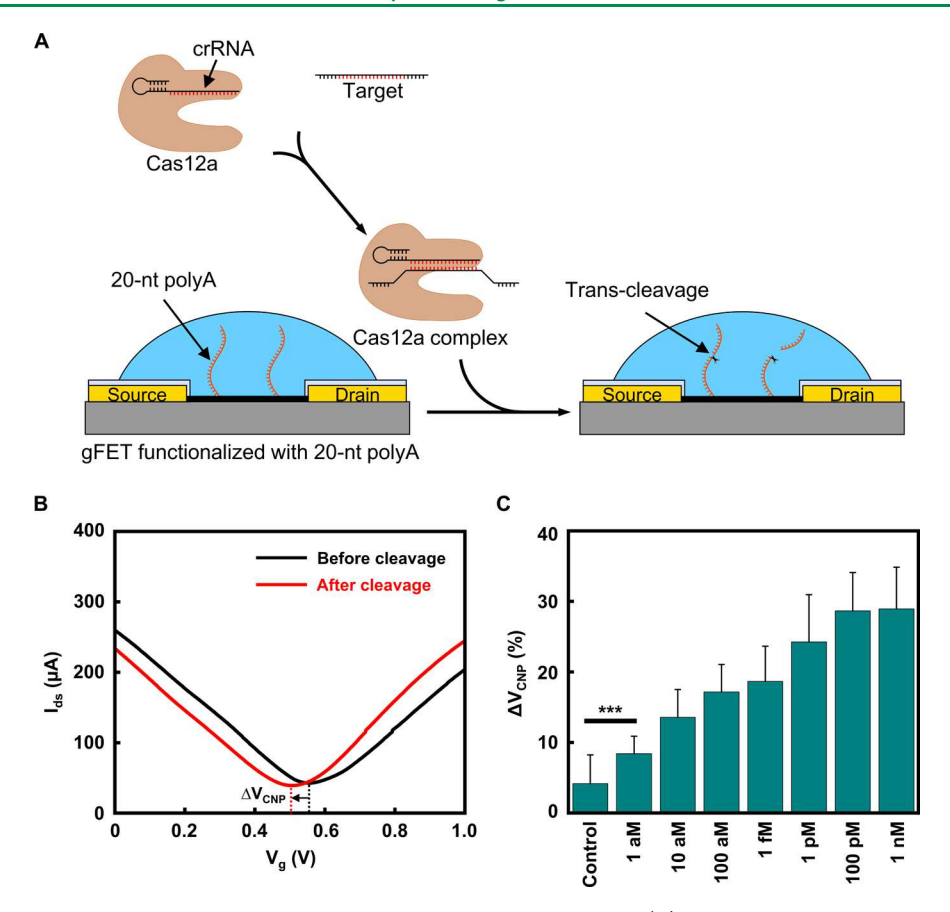


Figure 2. On-chip detection of ssDNA HPV-16 synthetic targets with attomolar sensitivity. (A) Cas12a-crRNA RNP complex binds with the DNA target, initiating trans-cleavage of 20-nt polyA probes tethered to the graphene surface. (B) Demonstration of  $V_{\rm CNP}$  shift for detection of the 1 fM HPV-16 synthetic target. (C) Shift in  $V_{\rm CNP}$  at different synthetic HPV-16 ssDNA target concentrations (control: n=18, 1 aM: n=20, 10 aM: n=26, 100 aM: n=38, 1 fM: n=28, \*\*\* p<0.001).

way to address strong variability is to harness the miniaturization capability of gFET by fabricating high-density devices within a small area and generate a large data set for accurate detection. Taking advantage of this design, our platform features an array of 48 gFETs on a single 1.5 cm  $\times$  1.5 cm Si/SiO<sub>2</sub> wafer chip (Figure 1C), with an active graphene sensing area of 80  $\mu$ m  $\times$  20  $\mu$ m (Figure 1D). Liquid gating using an Ag/AgCl electrode provides uniform electric field distribution and modulates charge carrier density in a relatively small gate voltage sweep range for transfer characteristics measurement. The biosensor array can generate a maximum of 48 data values for statistical analysis given a single 20  $\mu$ L CRISPR assay (1  $\mu$ L input sample). Compared with the majority of biosensor platforms, the 48-channel device offers an adequate statistical sample size to achieve a high level of measurement confidence. The small size of gFET allows biosensing applications where only a limited sample volume can be collected. To prevent parasitic source-drain current leakage, an SU-8 photoresist layer encapsulates graphene channels (Figure 1D). A total of 21 devices can be fabricated on a 4-inch wafer (Figure 1E), indicating the compatibility with large-scale manufacturing for potential distribution to the community.

On-Chip Detection of ssDNA HPV-16 Synthetic Targets. To first demonstrate the feasibility of the CRISPR Cas12a-gFET platform for ultrasensitive DNA detection, we used a previously reported Cas12a-crRNA-target-probe combination for amplification-free HPV-16 detection on an

electrochemical sensor. 42 Since target ssDNA complementary to crRNA is sufficient for the activation of Cas12a collateral activities, we intentionally employed single-stranded rather than double-stranded HPV-16 target sequence to demonstrate the versatility for ssDNA detection by our biosensor array. The Lachnospiraceae bacterium ND2006 Cas12a (LbCas12a)crRNA complex binds with HPV-16 ssDNA target sequence and cleaves 20-nt polyA probe sequence on the graphene surface (Figure 2A). The successful functionalization of PBASE linker to anchor 20-nt polyA probes is confirmed by a decrease in the intensity ratio of 2D to G Raman peak  $(I_{2D})$ I<sub>G</sub>) and right shifts of both G and 2D peaks from pristine graphene to PBASE-modified graphene due to the doping effect (Figure S1). A small peak at 1625.66 cm<sup>-1</sup> is attributed to pyrene group resonance through  $\pi - \pi$  stacking.<sup>58</sup> A representative measurement of transfer characteristics reveals a negative shift after the introduction of CRISPR assay containing 1 fM synthetic target (Figure 2B), corresponding to an increase in the electron carrier density after probe cleavage. The CRISPR Cas12a-gFET sensor could detect synthetic ssDNA HPV-16 target with an LOD of 1 aM (Figure 2C), and a linear relationship between the sensor response and the logarithmic concentrations of HPV-16 synthetic targets over a dynamic range of 1 aM to 100 pM was obtained (Figure S2), clearly showing the viability for ultrasensitive DNA detection free of target preamplification.

Nonpathogenic *E. coli* CRISPR Assay Development. Encouraged by the ultrasensitive detection of ssDNA targets,

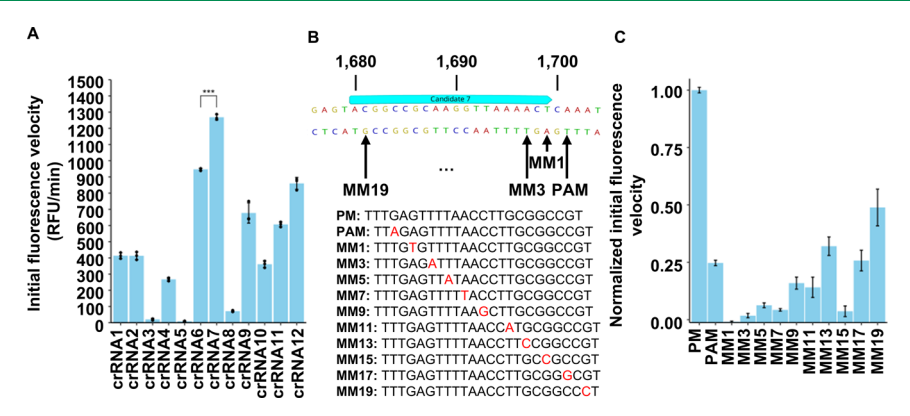


Figure 3. Screening of LbCas12a crRNAs targeting the 16S rRNA gene of E. coli. (A) Initial velocities of trans-cleavage activities are calculated for all 12 crRNAs from the first 10 min to screen for fast kinetics and short detection time. (B) Target site mismatches are shown compared to the perfect match. The red letter is the mismatched nucleotide. PM: perfect match. PAM: PAM mismatch. MM1: mismatch at nucleotide position 1. (C) Initial velocities of crRNA7 when detecting target sites with mismatches. All the data are normalized to the perfect match target site. For (A), data are represented as mean  $\pm$  s.d. from three technical replicates.

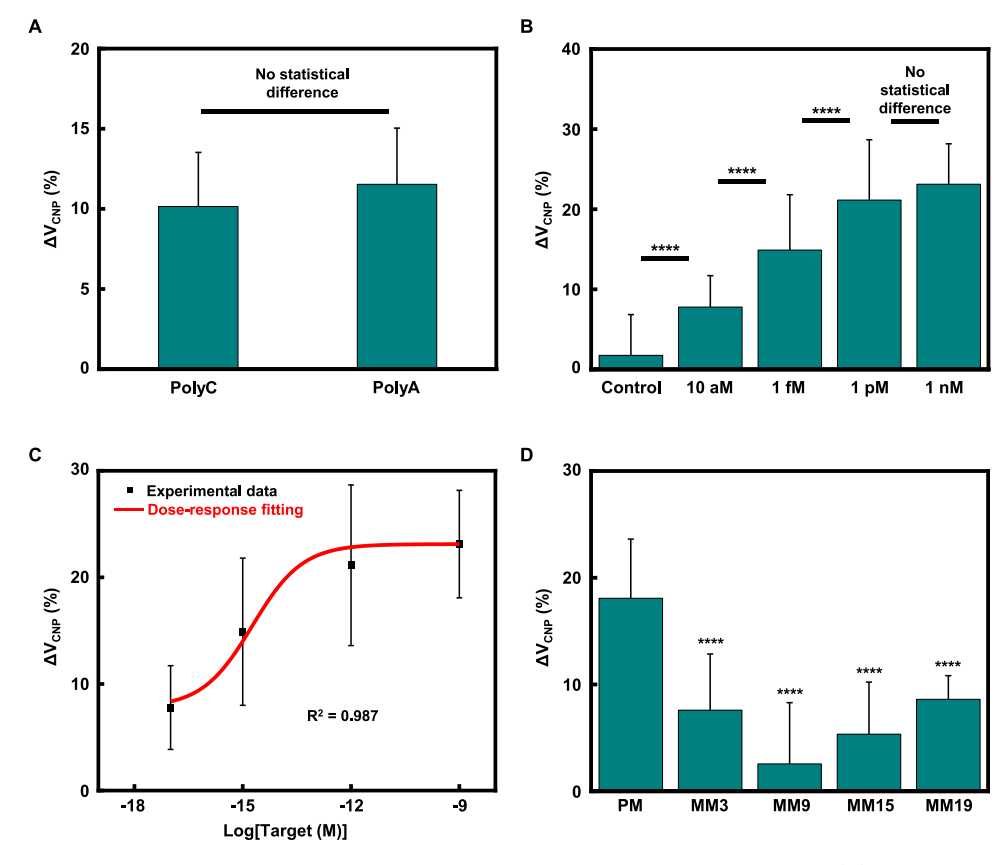


Figure 4. On-chip detection of dsDNA nonpathogenic *E. coli* plasmid targets using Cas12a-gFET arrays. (A) Comparison of 20-nt polyA and polyC probe for LbCas12a-mediated detection (polyC: n = 43, polyA: n = 45). (B) Shift in  $V_{\text{CNP}}$  at different *E. coli* target concentrations (control: n = 37, 10 aM: n = 47, 1 fM: n = 48, 1 pM: n = 36, 1 nM: n = 47, \*\*\*\* p < 0.0001). (C) Dose—response curve for the on-chip detection of nonpathogenic *E. coli* plasmid targets using the CRISPR Cas12a-gFET array. (D) Single-nucleotide polymorphisms (SNP) discrimination at 1 pM *E. coli* plasmid target concentration (PM: n = 27, MM3: n = 32, MM9: n = 7, MM15: n = 33, MM19: n = 45, \*\*\*\* p < 0.0001). The detailed target sequences for PM, MM3, MM9, MM15, and MM19 can be found in Figure 3B.

we wondered whether the CRISPR Cas12a-gFET could be used to detect dsDNA targets such as pathogenic bacterial DNAs. Pathogenic bacteria have caused many food recalls and disease outbreaks in the past decades. <sup>59–61</sup> A variety of conventional and novel methods can be applied to quickly and accurately identify the pathogenic bacteria species. <sup>62</sup> Among them, DNA sequencing and quantitative PCR are popular technologies based on the detection of nucleic acids. <sup>63</sup> In these

techniques, the 16S rRNA gene is often selected as the target DNA sequence when the contaminant is unknown because it exists in almost all bacterial species and has both highly conserved regions that help differentiate prokaryotes from eukaryotes and variable regions that are different across bacteria species and strains. These two regions allow for both the confirmation of bacteria presence and the initial identification of bacteria species. Hence, we selected non-

pathogenic E. coli (Migula) Castellani and Chalmers (Cat. No.: 25922; ATCC, Manassas, VA, USA) as a surrogate for pathogenic E. coli O157:H7 and retrieved its 16S rRNA gene from the National Center for Biotechnology Information (NCBI) database to find potential LbCas12a target sites with TTTV protospacer adjacent motif (PAM). We aligned these potential target sites to the genome of 12 common foodborne pathogens to only include E. coli-specific sequences. 65 To achieve high specificity, at least three mismatches are required between the E. coli target sites and the 12 foodborne pathogens. A total of 12 sites were found, and their corresponding LbCas12a CRISPR-RNAs (crRNA) were named from crRNA1 to crRNA12 (Table S2). Because different combinations of crRNA and complementary target site result in different trans-cleavage efficiencies, all 12 target sites were tested using a fluorescence-based plate reader assay.34 We subtracted background noises from raw fluorescence signals for each crRNA and compared their initial velocities (Figure 3A). Of all 12 candidates, nine crRNA-target pairs showed different levels of trans-cleavage activities, while the other three had little to no trans-cleavage. Among them, crRNA7 had the fastest kinetics and was chosen for further testing. To validate the applicability of the developed assay for quantitative measurement, we investigated the kinetics of LbCas12a collateral cleavage activity. The collateral cleavage of LbCas12a was found to be governed by Michaelis-Menten kinetics at a turnover rate of  $0.17 \text{ s}^{-1}$  and a catalytic efficiency of  $6.3 \times 10^5 \text{ M}^{-1} \text{ s}^{-1}$  (Figure S3), comparable to previously reported values. <sup>66,67</sup> Additionally, to ensure high specificity of crRNA7, a series of single-nucleotide mismatches was introduced to the target site but not the crRNA (Figure 3B). The crRNA7 had almost no activities when the mismatch was close to the PAM site from nucleotide 1 to 7 (Figure 3C). It was tolerant on most other nucleotide positions and had up to 50% of the perfect match activities. This level of mismatch tolerance is in good agreement with previous findings and shows high specificity of LbCas12a-based detection of E. coli using crRNA7.34

On-Chip Detection of dsDNA Nonpathogenic *E. coli* Plasmid Targets. Previous studies have reported that LbCas12a shows the highest trans-cleavage efficiency toward cytosine (C)-rich probes, <sup>67–69</sup> so we compared the collateral cleavage performance on 20-nt polyC and polyA sequence using our designed CRISPR-Cas12a *E. coli* assay and gFET array. PBASE functionalization contributes to a right shift in transfer characteristics due to the electron-withdrawing property by the ester group, and polyC probe immobilization induces a further positive shift mainly due to the increased gating effect from negative charges in DNA backbones (Figure S4). Using the same *E. coli* plasmid concentration (1 fM final concentration in assay), we observed a similar trans-cleavage response toward these probes (polyC 10.15% vs. polyA 11.53%, Figure 4A), probably due to the the saturation of trans-cleavage response after 30 min assay incubation time.

To demonstrate the flexibility of the Cas12a-gFET on probe choice, we used 20-nt polyC probes in subsequent experiments. We added serial dilutions of *E. coli* target plasmids into Cas12a assay and determined the LOD to be 10 aM, and meanwhile, the detection signals reached saturation at 1 nM with a change of 23.12% (Figure 4B). Fitting the CNP voltage shift at different logarithmic concentrations of *E. coli* plasmid into a dose—response relationship generated a calibration curve (Figure 4C). It should be noted that although the

conformation of Cas12a RNP complex is stabilized by the nontarget strand of a dsDNA target, thus favoring transcleavage activated by dsDNA,<sup>34</sup> the potential difference in the trans-cleavage efficiency between the *E. coli* plasmid and synthetic HPV-16 ssDNA assays may shed light on the decreased sensitivity in this case.

To investigate the capability of the CRISPR Cas12a-gFET platform to distinguish SNPs, we tested our platform against the perfect match target and four single-mismatch off-targets. We selected MM19, which showed the highest off-target collateral cleavage activity (Figure 3C), and three mismatches across different positions in the target region (MM3, MM9, and MM15). Since SNP discrimination has been validated with other mismatch targets in fluorescence-based detection (Figure 3C), we believe four mismatch targets should be sufficient to generalize the SNP detection capability of our platform. We measured the signal responses of CRISPR Cas12a-gFET using 1 pM mismatched targets to investigate the Cas12a collateral activity on this platform at a high concentration of off-targets. All mismatched crRNA-target pairs, despite causing changes in CNP voltage, generated shifts significantly lower than the signal response from the perfect match target (Figure 4D), indicating the high specificity of CRISPR Cas12a-gFET in differentiating SNPs.

## DISCUSSION

Overall, we have demonstrated a CRISPR-Cas12a-mediated gFET platform for amplification-free and reliable DNA detection with attomolar sensitivity and single-nucleotide selectivity. This CRISPR Cas12a-gFET array is among the most sensitive amplification-free CRISPR-based DNA detection platforms to date (LOD: 1 aM for ssDNA HPV-16 and 10 aM for dsDNA nonpathogenic E. coli plasmid target; 30 min incubation time at room temperature), therefore satisfying more stringent clinical requirements when only a small amount of target DNA is present; 70 it is at least two orders of magnitude more sensitive than the Cas9-based CRISPR-Chip gFET biosensor (LOD: 1.7 fM)<sup>31</sup> and six orders of magnitude more sensitive than the E-CRISPR platform (LOD: 50 pM), which integrates the trans-cleavage activity of CRISPR Cas12a with conventional electrochemical sensors.<sup>42</sup> Additionally, compared with the Cas9-based CRISPR-Chip gFET biosensor, 31,32 our device is able to expand the DNA targeting capacity beyond dsDNA and include ssDNA. To cope with the identification of diverse DNA targets, CRISPR-Chip requires the immobilization of different target-specific dCas9-gRNA complexes to the device surface. Similarly, a recent hybridization-based gFET biosensor for attomolar DNA detection and SNP discrimination<sup>71</sup> has to change the probe DNA sequence immobilized on the graphene surface if the detection of a different target is desired. In contrast, the preparation of our CRISPR Cas12a-gFET transducer components is streamlined and only the crRNA sequence in the solution-based assay needs to be changed. Thus, the CRISPR Cas12a-gFET is a universal DNA detection platform highly suitable for largescale production and widespread distribution.

Furthermore, as opposed to other amplification-free CRISPR-derived DNA detection platforms with attomolar sensitivity, 47,69 the Cas12a-gFET relies on electrical measurements, avoiding the need for expensive optical modules for fluorescence or Raman measurements. Our device can potentially be integrated with miniaturized electronics for data acquisition, thus realizing point-of-care testing. We also

show that our Cas12a-gFET system is highly specific and capable of detecting SNPs. This allows a wider range of applications for the identification of pathogen variants and disease-related gene mutations rather than merely discrimination of different species. In addition, our gFET platform holds promise for clinical diagnostics, which has been validated in our CRISPR Cas13a-gFET to detect clinical SARS-CoV-2 samples. 44 More importantly, ssDNA probes immobilized on a gold electrode are stable for CRISPR-mediated electrochemical detection for approximately 3 days when stored at 4  $^{\circ}\text{C}$  in a humid chamber. 42 Combining with lyophilization of CRISPR reagents,<sup>72</sup> the preparation of devices and assays can be potentially decoupled from the detection process, thus facilitating field deployment. Overall, we have demonstrated an ultrasensitive, reliable, highly specific, and target amplification-free DNA detection platform that can be readily adapted for diverse applications.

## MATERIALS AND METHODS

Design of crRNA for Nonpathogenic E. coli Detection. The DNA sequence of E. coli 16S rRNA was retrieved from the NCBI database (https://www.ncbi.nlm.nih.gov/). TTTV sites were identified, and the 20 nucleotides downstream of these PAM sites were selected as potential target sites. All target sites were compared with the whole genome of 12 common foodborne pathogens, including Campylobacter jejuni, Enterococcus faecalis, Listeria ivanovii, Listeria monocytogenes, Proteus mirabilis, Salmonella enterica, Shigella dysenteriae, Staphylococcus aureus, Streptococcus pyogenes, Vibrio fluvialis, Vibrio parahaemolyticus, and Yersinia enterocolitica, through BLAST (https://blast.ncbi.nlm.nih.gov/Blast.cgi). Any target sites with fewer than three mismatches were excluded.

Construction of Nonpathogenic E. coli and crRNA Plasmids. Primers were ordered from Integrated DNA Technologies (IDT, Coralville, IA, USA). E. coli 16S rRNA DNA sequence was cloned from American Type Culture Collection (ATCC, Manassas, VA, USA) E. coli strain 25922. LbCas12a crRNAs were ordered as overlapping primers and later extended and cloned downstream of a T7 promoter (pLSB-NAT, plasmid #166698; Addgene, Watertown, MA, USA) via Golden Gate cloning (Cat. No.: E1601L; New England Biolabs, Ipswich, MA, USA). Plasmids were transformed into Stbl3 competent E. coli cells (Cat. No.: C737303; Thermo Fisher Scientific, Waltham, MA, USA). Transformed cells were streaked on ampicillin LB agar plates and incubated at 37 °C overnight. Single colonies were selected and grown in 5 mL LB culture media supplied with ampicillin overnight at  $37\,^{\circ}\text{C}$  at  $280\,\text{rpm}$ . The plasmid was extracted using QIAprep Spin Miniprep kit following the manufacturer's instructions (Cat. No.: 27104; QIAGEN, Hilden, Germany). The plasmid sequence was confirmed by Sanger Sequencing (GENEWIZ, South Plainfield, NJ, USA).

In Vitro Transcription of crRNA. The desired fragments containing the T7 promoter, direct repeat, and spacer sequence were PCR amplified from the plasmids and purified using the QIAquick Gel Extraction kit (Cat. No.: 28704; QIAGEN, Hilden, Germany). The crRNA was transcribed in vitro using HiScribe T7 Quick High Yield RNA Synthesis kit (Cat. No.: E2050S; New England Biolabs, Ipswich, MA, USA) and purified using VAHTS RNA clean beads (Cat. No.: N412-02; Vazyme, Nanjing, Jiangsu, China). The RNA products were aliquoted into PCR tubes and stored at -80 °C until use. All procedures followed manufacturers' instructions.

Validation of CRISPR Assay by Fluorescence Detection. The collateral activities of LbCas12a proteins (Cat. No.: M0653T; New England Biolabs, Ipswich, MA, USA) were tested using a fluorescence-based assay. The LbCas12a proteins and crRNAs were first incubated at 37 °C for 15 min to form RNP complexes. The targets and the reporters were subsequently added into the reaction mixture to initiate the reaction. The samples were quickly mixed and transferred to a 384-well plate (Cat. No.: 3820; Corning Inc., Corning, NY, USA) by pipetting. The final concentration was 50 nM

LbCas12a protein, 62.5 nM crRNA, 250 pM target plasmid, 1× NEB r2.1 buffer (Cat. No.: B6002S; New England Biolabs, Ipswich, MA, USA), and 50 nM DNase Alert reporters (Cat. No.: 11-04-02-03; IDT, Coralville, IA, USA) in a 20  $\mu$ L reaction or the same composition without the target plasmid for no template controls. The fluorescence signals were measured every minute ( $\lambda_{\rm ex} = 526$  nm,  $\lambda_{\rm em} = 556$  nm, gain = 150) using a microplate reader (Model: Infinite M200; Tecan Group Ltd., Männedorf, Switzerland).

**Fabrication of 48-Channel gFETs.** The fabrication of a 48-channel gFET array can be divided into three steps: (1) preparation of source—drain contact pads, (2) transfer of graphene sheet and patterning of 48 graphene channels, and (3) encapsulation to reduce source—drain current leakage. An overview of the fabrication process is provided in Figure S5, and the detailed protocols can be found in Supplementary Note 1.

The patterning of source-drain contact pads followed the standard photolithography process in combination with thin film deposition. Briefly, AZ 5214E photoresist (MicroChemicals GmbH, Ulm, Germany) was spin-cast onto a Si/SiO<sub>2</sub> wafer, followed by prebaking at 110 °C for 3 min. The photoresist was exposed under a 365 nm LED light source using a maskless aligner (Model:  $\mu$ MLA; Heidelberg Instruments, Heidelberg, Germany), and the entire wafer was immersed in a solution of 1:4 (v/v) AZ 400 K developer (MicroChemicals GmbH, Ulm, Germany): deionized (DI) water for 25 s. The developing process was stopped by rinsing with DI water, thereby forming desired microscale patterns ready for thin film deposition. Sequential sputtering (Model: A300; AJA International, Inc., MA, USA) of 15 nm chromium (Cr) or titanium (Ti) adhesion layer and 90 nm gold (Au) layer, along with subsequent lift-off of the photoresist by soaking in acetone (Sigma-Aldrich, St. Louis, MO, USA) for 1 h, resulted in source-drain gold electrodes for gFETs.

Following the fabrication of contact pads, a monolayer of graphene film was transferred onto the device based on a poly(methyl methacrylate) (PMMA)-assisted method. 44,73 A droplet of PMMA A4 solution (4-wt % PMMA dissolved in anisole, Sigma-Aldrich, St. Louis, MO, USA) was allowed to spread over CVD-grown graphene on copper foil (Graphenea, Cambridge, MA, USA). After evaporation of anisole, the PMMA-covered graphene film on the copper foil substrate was placed in the copper etchant for approximately 30 min and transferred, using a clean wafer chip as a substrate, into dilute hydrochloric acid (HCl, three droplets of 1 M HCl in ~300 mL DI water; Sigma-Aldrich, St. Louis, MO, USA) to remove residual copper etchant. The graphene film was then transferred to DI water to remove HCl, and this step was repeated twice. Subsequently, the clean graphene film was transferred onto a set of patterned gold electrodes. After water evaporation, a droplet of PMMA A2 solution (2-wt % PMMA in anisole) was added to relax the wrinkled graphene film, and again, the anisole was allowed to evaporate. The wafer was soaked in acetone for 1 h to remove PMMA, and the standard photolithography process as previously described in the contact pad fabrication was applied to define graphene patterns. Finally, the unwanted regions of the graphene films were completely etched away by oxygen plasma (Model: Tergeo Plus; PIE Scientific LLC, Union City, CA, USA), and the AZ 5214E photoresist was removed by soaking the wafer in acetone for 1 h.

To reduce current leakage, an encapsulation layer made of SU-8 2000.5 photoresist (Kayaku Advanced Materials, Westborough, MA, USA) was formed by photolithography. The photoresist was spin cast onto the as-prepared gFETs and prebaked at 110 °C for 1 min. After the exposure, the photoresist was postbaked at 110 °C for 4 min. An encapsulation pattern was generated by immersing the wafer in SU-8 developer (Kayaku Advanced Materials, Westborough, MA, USA) for 1 min and rinsing with isopropanol (Sigma-Aldrich, St. Louis, MO, USA). The fabricated gFET arrays were cut into individual 1.5 cm  $\times$  1.5 cm chips using a diamond scribe.

Functionalization of DNA Probes on the Graphene Surface. A gFET chip was immersed in a 2 mM or 5 mM 1-pyrenebutyric acid N-hydroxysuccinimide ester (PBASE; Sigma-Aldrich, St. Louis, MO, USA) solution in methanol (Sigma-Aldrich, St. Louis, MO, USA) in a chamber with methanol for 2 h. The chip was then rinsed with

methanol and DNase/RNase-free distilled water (Invitrogen, Waltham, MA, USA) and incubated in 1  $\mu$ M amino-modified 20-nt poly-C probes (/SAmMC6/CC CCC CCC CCC CCC CCC CCC; IDT, Coralville, IA, USA) in a humid chamber with nuclease-free water for 2 h. After rinsing with nuclease-free water, the unreacted PBASE linkers were quenched by 1 mM amino-PEG5-alcohol (BroadPharm, San Diego, CA, USA) in a humid chamber for 10 min and 1 M ethanolamine hydrochloride (Sigma-Aldrich, St. Louis, MO, USA) in a humid chamber for another 10 min to prevent nonspecific adsorption during CRISPR reaction.

Detection of Nonpathogenic *E. coli* and HPV-16 by Cas12-Mediated gFET. The Cas12a crRNA-target pair for HPV-16 detection has been previously reported and ordered from IDT. To demonstrate the versatility of CRISPR-mediated gFET for both ssDNA and dsDNA detection, we intentionally used a single-stranded HPV-16 target sequence. The CRISPR-Cas12a crRNA and nonpathogenic *E. coli* target plasmid were prepared as previously discussed. For on-chip CRISPR reaction, an amplification-free assay consisting of LbCas12a, crRNA, synthetic DNA target, nuclease-free water, HEPES buffer (Invitrogen, Waltham, MA, USA), and magnesium chloride solution (MgCl<sub>2</sub>; Invitrogen, Waltham, MA, USA) was applied to the probe-functionalized gFET array. A 20  $\mu$ L CRISPR assay was assembled as shown in Table 1 below.

Table 1. CRISPR-Cas12a Assay for Nonpathogenic E. coli and HPV-16 Detection

step	reagent	volume $(\mu L)$
1	nuclease-free water	13.8
2	HEPES buffer (1 M)	0.4
3	MgCl <sub>2</sub> (50 mM)	3.6
4	LbCas12a (1 $\mu$ M in NEB r2.1 buffer)	0.6
5	E. coli or HPV-16 crRNA (1 $\mu$ M in nuclease-free water)	0.6
6	incubate in the dark at room temperature for 10 min	
7	E. coli or HPV-16 synthetic DNA target (20× final concentration)	1
8	incubate in the dark at room temperature for 10 min	

For transfer characteristics measurement, the gFET array was gated by 2 mM MgCl $_2$  solution or 1× phosphate-buffered saline (PBS, pH 7.4; Invitrogen, Waltham, MA, USA) with a silver/silver chloride (Ag/AgCl) gate electrode. Using a semiconductor device analyzer (Model: B1500A; Keysight Technologies, Santa Rosa, CA, USA), the transfer characteristics were recorded by sweeping the gate voltage from -1 to 1 V with a step size of 1 mV under a 100 mV source—drain bias voltage.

Prior to the measurement of transfer characteristics, whether preor postcleavage, the probe-functionalized gFET chip was incubated in 40  $\mu\rm L$  test solution (2 mM MgCl<sub>2</sub> or 1× PBS) for 15 min to soak the graphene channels with the test solution for stable signal responses and then rinsed with the test solution to remove loosely bound blocking agents (precleavage) or residual cleaved probes (postcleavage). Therefore, the gFET array was ready for measurement when another 40  $\mu\rm L$  test solution was added. After recording precleavage transfer characteristics, the chip was rinsed with nuclease-free water. The CRISPR-Cas12a assay, as prepared in Table 1, was applied to the chip followed by incubation in the dark at room temperature in a humid chamber for 30 min. Finally, the chip was washed with nuclease-free water to remove the assay, and postcleavage transfer characteristics were measured after the incubation and rinsing procedure.

## ASSOCIATED CONTENT

## Supporting Information

The Supporting Information is available free of charge at https://pubs.acs.org/doi/10.1021/acssensors.2c02495.

Protocols for the fabrication of gFETs, Raman characterization of PBASE functionalization, calibration curve for the on-chip detection of HPV-16 ssDNA targets using CRISPR Cas12a-gFET array, kinetics of LbCas12a collateral cleavage, transfer characteristics of PBASE and probe functionalization, schematic illustration of the fabrication process, comparison of different CRISPR-based amplification-free DNA detection platforms, and sequences of DNA and RNA oligonucleotides used in this study (PDF)

## AUTHOR INFORMATION

## **Corresponding Authors**

Xue Gao − Department of Chemical and Biomolecular Engineering, Department of Bioengineering, and Department of Chemistry, Rice University, Houston, Texas 77005, United States; orcid.org/0000-0003-3213-9704; Email: xue.gao@rice.edu

Yi Zhang — Department of Biomedical Engineering and Institute of Materials Science, University of Connecticut, Storrs, Connecticut 06269, United States; oocid.org/0000-0002-0907-663X; Email: yi.5.zhang@uconn.edu

#### **Authors**

Zhengyan Weng — Department of Biomedical Engineering and Institute of Materials Science, University of Connecticut, Storrs, Connecticut 06269, United States

Zheng You — Department of Chemical and Biomolecular Engineering, Rice University, Houston, Texas 77005, United States

Huijie Li — Department of Biomedical Engineering and Institute of Materials Science, University of Connecticut, Storrs, Connecticut 06269, United States; orcid.org/0000-0002-8304-5241

Guangfu Wu – Department of Biomedical Engineering and Institute of Materials Science, University of Connecticut, Storrs, Connecticut 06269, United States

Yang Song — Department of Biomedical Engineering and Institute of Materials Science, University of Connecticut, Storrs, Connecticut 06269, United States; orcid.org/0000-0003-0626-0850

He Sun − Department of Biomedical Engineering and Institute of Materials Science, University of Connecticut, Storrs, Connecticut 06269, United States; orcid.org/0000-0003-3701-9453

Ava Fradlin – Department of Kinesiology, Rice University, Houston, Texas 77005, United States

Camille Neal-Harris — Department of Bioengineering and Department of Visual and Dramatic Arts, Rice University, Houston, Texas 77005, United States

Mengshi Lin − Food Science Program, Division of Food, Nutrition & Exercise Sciences, University of Missouri, Columbia, Missouri 65211, United States; orcid.org/ 0000-0002-6967-2257

Complete contact information is available at: https://pubs.acs.org/10.1021/acssensors.2c02495

## **Author Contributions**

<sup>T</sup>Z.W., Z.Y., and H.L. contributed equally to this study.

#### Notes

The authors declare no competing financial interest.

Experimental data are expressed as the mean  $\pm$  standard derivation (SD). One-way ANOVA with Tukey's test is used for significance analysis. The software used for statistical analysis is OriginPro 2022.

All data needed to evaluate the conclusions in the study are present in the paper and/or the Supplementary Information.

## ACKNOWLEDGMENTS

We acknowledge the funding support by the University of Connecticut start-up fund (to Y.Z.), NSF CBET-2103025 and ECCS-2113736 (to Y.Z.), Rice University startup fund (to X.G.), NSF CBET-2031242 (to X.G.), and Welch Foundation C-1952 (to X.G.).

## REFERENCES

- (1) Weiss, J. B. DNA probes and PCR for diagnosis of parasitic infections. *Clin. Microbiol. Rev.* **1995**, *8*, 113–130.
- (2) Sidransky, D. Nucleic acid-based methods for the detection of cancer. *Science* **1997**, 278, 1054–1058.
- (3) Green, C.; Huggett, J. F.; Talbot, E.; Mwaba, P.; Reither, K.; Zumla, A. I. Rapid diagnosis of tuberculosis through the detection of mycobacterial DNA in urine by nucleic acid amplification methods. *Lancet Infect. Dis.* **2009**, *9*, 505–511.
- (4) Polina, I. A.; Ilatovskaya, D. V.; DeLeon-Pennell, K. Y. Cell free DNA as a diagnostic and prognostic marker for cardiovascular diseases. *Clin. Chim. Acta* **2020**, *503*, 145–150.
- (5) Saluja, H.; Karapetis, C. S.; Pedersen, S. K.; Young, G. P.; Symonds, E. L. The Use of Circulating Tumor DNA for Prognosis of Gastrointestinal Cancers. *Front. Oncol.* **2018**, *8*, 275.
- (6) Valsamakis, A. Molecular testing in the diagnosis and management of chronic hepatitis B. *Clin. Microbiol. Rev.* **2007**, *20*, 426–439.
- (7) Sanz-Garcia, E.; Zhao, E.; Bratman, S. V.; Siu, L. L. Monitoring and adapting cancer treatment using circulating tumor DNA kinetics: Current research, opportunities, and challenges. *Sci. Adv.* **2022**, *8*, No. eabi8618.
- (8) Xia, X.; Yang, H.; Cao, J.; Zhang, J.; He, Q.; Deng, R. Isothermal nucleic acid amplification for food safety analysis. *TrAC Trends Anal. Chem.* **2022**, *153*, No. 116641.
- (9) Li, F.; Peng, Y.; Fang, W.; Altermatt, F.; Xie, Y.; Yang, J.; Zhang, X. Application of Environmental DNA Metabarcoding for Predicting Anthropogenic Pollution in Rivers. *Environ. Sci. Technol.* **2018**, *52*, 11708–11719.
- (10) Malla, B.; Haramoto, E. Host-specific mitochondrial DNA markers for tracking the sources of fecal pollution. *Curr. Opin. Environ. Sci. Health* **2020**, *16*, 34–46.
- (11) Bohmann, K.; Evans, A.; Gilbert, M. T.; Carvalho, G. R.; Creer, S.; Knapp, M.; Yu, D. W.; de Bruyn, M. Environmental DNA for wildlife biology and biodiversity monitoring. *Trends Ecol. Evol.* **2014**, 29, 358–367.
- (12) Sperry, B. P.; Allyse, M.; Sharp, R. R. Genetic Fingerprints and National Security. *Am. J. Bioeth.* **2017**, *17*, 1–3.
- (13) McCord, B. R.; Gauthier, Q.; Cho, S.; Roig, M. N.; Gibson-Daw, G. C.; Young, B.; Taglia, F.; Zapico, S. C.; Mariot, R. F.; Lee, S. B.; et al. Forensic DNA Analysis. *Anal. Chem.* **2019**, *91*, *673*–688.
- (14) Petralia, S.; Conoci, S. PCR Technologies for Point of Care Testing: Progress and Perspectives. ACS Sens. 2017, 2, 876-891.
- (15) Zhong, J.; Zhao, X. Isothermal Amplification Technologies for the Detection of Foodborne Pathogens. *Food Anal. Methods* **2018**, *11*, 1543–1560.
- (16) Xia, L.; Zhuang, J.; Zou, Z.; Yin, J.; Mu, Y. Direct digital polymerase chain reaction chip for the detection of EGFR T790M mutation in plasma. *Talanta* **2022**, 237, No. 122977.
- (17) Li, F. W.; Kuo, L. Y.; Huang, Y. M.; Chiou, W. L.; Wang, C. N. Tissue-direct PCR, a rapid and extraction-free method for barcoding of ferns. *Mol. Ecol. Resour.* **2010**, *10*, 92–95.

- (18) Astbury, S.; Costa Nunes Soares, M. M.; Peprah, E.; King, B.; Jardim, A. C. G.; Shimizu, J. F.; Jalal, P.; Saeed, C. H.; Sabeer, F. T.; Irving, W. L.; Tarr, A. W.; McClure, C. P. Nanopore sequencing from extraction-free direct PCR of dried serum spots for portable hepatitis B virus drug-resistance typing. *J. Clin. Virol.* **2020**, *129*, No. 104483.
- (19) Zai, Y.; Min, C.; Wang, Z.; Ding, Y.; Zhao, H.; Su, E.; He, N. A sample-to-answer, quantitative real-time PCR system with low-cost, gravity-driven microfluidic cartridge for rapid detection of SARS-CoV-2, influenza A/B, and human papillomavirus 16/18. *Lab Chip* **2022**, 22, 3436.
- (20) Liu, W.; Yue, F.; Lee, L. P. Integrated Point-of-Care Molecular Diagnostic Devices for Infectious Diseases. *Acc. Chem. Res.* **2021**, *54*, 4107–4119.
- (21) Czilwik, G.; Messinger, T.; Strohmeier, O.; Wadle, S.; von Stetten, F.; Paust, N.; Roth, G.; Zengerle, R.; Saarinen, P.; Niittymaki, J.; et al. Rapid and fully automated bacterial pathogen detection on a centrifugal-microfluidic LabDisk using highly sensitive nested PCR with integrated sample preparation. *Lab Chip* **2015**, *15*, 3749–3759.
- (22) Yin, J.; Suo, Y.; Zou, Z.; Sun, J.; Zhang, S.; Wang, B.; Xu, Y.; Darland, D.; Zhao, J. X.; Mu, Y. Integrated microfluidic systems with sample preparation and nucleic acid amplification. *Lab Chip* **2019**, *19*, 2769–2785.
- (23) Taylor, S. M.; Juliano, J. J.; Trottman, P. A.; Griffin, J. B.; Landis, S. H.; Kitsa, P.; Tshefu, A. K.; Meshnick, S. R. Highthroughput pooling and real-time PCR-based strategy for malaria detection. *J. Clin. Microbiol.* **2010**, *48*, 512–519.
- (24) Makrigiorgos, G. M.; Chakrabarti, S.; Zhang, Y.; Kaur, M.; Price, B. D. A PCR-based amplification method retaining the quantitative difference between two complex genomes. *Nat. Biotechnol.* **2002**, *20*, 936–939.
- (25) Bustin, S. A.; Benes, V.; Garson, J.; Hellemans, J.; Huggett, J.; Kubista, M.; Mueller, R.; Nolan, T.; Pfaffl, M. W.; Shipley, G.; et al. The need for transparency and good practices in the qPCR literature. *Nat. Methods* **2013**, *10*, 1063–1067.
- (26) Hayden, R. T.; Hokanson, K. M.; Pounds, S. B.; Bankowski, M. J.; Belzer, S. W.; Carr, J.; Diorio, D.; Forman, M. S.; Joshi, Y.; Hillyard, D.; et al. Multicenter comparison of different real-time PCR assays for quantitative detection of Epstein-Barr virus. *J. Clin. Microbiol.* **2008**, *46*, 157–163.
- (27) Kelley, S. O. What Are Clinically Relevant Levels of Cellular and Biomolecular Analytes? *ACS Sens.* **2017**, *2*, 193–197.
- (28) Barrangou, R.; Fremaux, C.; Deveau, H.; Richards, M.; Boyaval, P.; Moineau, S.; Romero, D. A.; Horvath, P. CRISPR provides acquired resistance against viruses in prokaryotes. *Science* **2007**, *315*, 1709–1712.
- (29) Qian, S.; Chen, Y.; Xu, X.; Peng, C.; Wang, X.; Wu, H.; Liu, Y.; Zhong, X.; Xu, J.; Wu, J. Advances in amplification-free detection of nucleic acid: CRISPR/Cas system as a powerful tool. *Anal. Biochem.* **2022**, *643*, No. 114593.
- (30) Jinek, M.; Chylinski, K.; Fonfara, I.; Hauer, M.; Doudna, J. A.; Charpentier, E. A programmable dual-RNA-guided DNA endonuclease in adaptive bacterial immunity. *Science* **2012**, *337*, 816–821.
- (31) Hajian, R.; Balderston, S.; Tran, T.; deBoer, T.; Etienne, J.; Sandhu, M.; Wauford, N. A.; Chung, J. Y.; Nokes, J.; Athaiya, M.; et al. Detection of unamplified target genes via CRISPR-Cas9 immobilized on a graphene field-effect transistor. *Nat. Biomed. Eng.* **2019**, *3*, 427–437.
- (32) Balderston, S.; Taulbee, J. J.; Celaya, E.; Fung, K.; Jiao, A.; Smith, K.; Hajian, R.; Gasiunas, G.; Kutanovas, S.; Kim, D.; et al. Discrimination of single-point mutations in unamplified genomic DNA via Cas9 immobilized on a graphene field-effect transistor. *Nat. Biomed. Eng.* **2021**, *5*, 713–725.
- (33) Ma, E.; Harrington, L. B.; O'Connell, M. R.; Zhou, K.; Doudna, J. A. Single-Stranded DNA Cleavage by Divergent CRISPR-Cas9 Enzymes. *Mol. Cell* **2015**, *60*, 398–407.
- (34) Chen, J. S.; Ma, E.; Harrington, L. B.; Da Costa, M.; Tian, X.; Palefsky, J. M.; Doudna, J. A. CRISPR-Cas12a target binding unleashes indiscriminate single-stranded DNase activity. *Science* **2018**, *360*, 436–439.

- (35) Nalefski, E. A.; Patel, N.; Leung, P. J. Y.; Islam, Z.; Kooistra, R. M.; Parikh, I.; Marion, E.; Knott, G. J.; Doudna, J. A.; Le Ny, A. M.; et al. Kinetic analysis of Cas12a and Cas13a RNA-Guided nucleases for development of improved CRISPR-Based diagnostics. *iScience* **2021**, 24, No. 102996.
- (36) Sternberg, S. H.; Redding, S.; Jinek, M.; Greene, E. C.; Doudna, J. A. DNA interrogation by the CRISPR RNA-guided endonuclease Cas9. *Nature* **2014**, *507*, 62–67.
- (37) Choi, J. H.; Lim, J.; Shin, M.; Paek, S. H.; Choi, J. W. CRISPR-Cas12a-Based Nucleic Acid Amplification-Free DNA Biosensor via Au Nanoparticle-Assisted Metal-Enhanced Fluorescence and Colorimetric Analysis. *Nano Lett.* **2021**, *21*, 693–699.
- (38) He, Q.; Yu, D.; Bao, M.; Korensky, G.; Chen, J.; Shin, M.; Kim, J.; Park, M.; Qin, P.; Du, K. High-throughput and all-solution phase African Swine Fever Virus (ASFV) detection using CRISPR-Cas12a and fluorescence based point-of-care system. *Biosens. Bioelectron.* **2020**. *154*. No. 112068.
- (39) Yu, T.; Zhang, S.; Matei, R.; Marx, W.; Beisel, C. L.; Wei, Q. Coupling smartphone and CRISPR—Cas12a for digital and multiplexed nucleic acid detection. *AIChE J.* **2021**, *67*, No. e17365.
- (40) Liu, P. F.; Zhao, K. R.; Liu, Z. J.; Wang, L.; Ye, S. Y.; Liang, G. X. Cas12a-based electrochemiluminescence biosensor for target amplification-free DNA detection. *Biosens. Bioelectron.* **2021**, *176*, No. 112954.
- (41) Pang, Y.; Li, Q.; Wang, C.; Zhen, S.; Sun, Z.; Xiao, R. CRISPR-cas12a mediated SERS lateral flow assay for amplification-free detection of double-stranded DNA and single-base mutation. *Chem. Eng. J.* **2022**, *429*, No. 132109.
- (42) Dai, Y.; Somoza, R. A.; Wang, L.; Welter, J. F.; Li, Y.; Caplan, A. I.; Liu, C. C. Exploring the Trans-Cleavage Activity of CRISPR-Cas12a (cpf1) for the Development of a Universal Electrochemical Biosensor. *Angew. Chem., Int. Ed.* **2019**, *58*, 17399–17405.
- (43) Nouri, R.; Jiang, Y.; Lian, X. L.; Guan, W. Sequence-Specific Recognition of HIV-1 DNA with Solid-State CRISPR-Cas12a-Assisted Nanopores (SCAN). ACS Sens. 2020, 5, 1273–1280.
- (44) Li, H.; Yang, J.; Wu, G.; Weng, Z.; Song, Y.; Zhang, Y.; Vanegas, J. A.; Avery, L.; Gao, Z.; Sun, H.; Chen, Y.; Dieckhaus, K. D.; Gao, X.; Zhang, Y. Amplification-Free Detection of SARS-CoV-2 and Respiratory Syncytial Virus Using CRISPR Cas13a and Graphene Field-Effect Transistors. *Angew. Chem., Int. Ed.* **2022**, *61*, No. e202203826.
- (45) Yang, J.; Song, Y.; Deng, X.; Vanegas, J. A.; You, Z.; Zhang, Y.; Weng, Z.; Avery, L.; Dieckhaus, K. D.; Peddi, A.; Gao, Y.; Zhang, Y.; Gao, X. Engineered LwaCas13a with enhanced collateral activity for nucleic acid detection. *Nat. Chem. Biol.* **2023**, *19*, 45–54.
- (46) Kim, H.; Lee, S.; Seo, H. W.; Kang, B.; Moon, J.; Lee, K. G.; Yong, D.; Kang, H.; Jung, J.; Lim, E. K.; et al. Clustered Regularly Interspaced Short Palindromic Repeats-Mediated Surface-Enhanced Raman Scattering Assay for Multidrug-Resistant Bacteria. *ACS Nano* 2020, 14, 17241–17253.
- (47) Choi, J. H.; Shin, M.; Yang, L.; Conley, B.; Yoon, J.; Lee, S. N.; Lee, K. B.; Choi, J. W. Clustered Regularly Interspaced Short Palindromic Repeats-Mediated Amplification-Free Detection of Viral DNAs Using Surface-Enhanced Raman Spectroscopy-Active Nanoarray. ACS Nano 2021, 15, 13475—13485.
- (48) Zetsche, B.; Gootenberg, J. S.; Abudayyeh, O. O.; Slaymaker, I. M.; Makarova, K. S.; Essletzbichler, P.; Volz, S. E.; Joung, J.; van der Oost, J.; Regev, A.; et al. Cpf1 is a single RNA-guided endonuclease of a class 2 CRISPR-Cas system. *Cell* **2015**, *163*, 759–771.
- (49) Fonfara, I.; Richter, H.; Bratovic, M.; Le Rhun, A.; Charpentier, E. The CRISPR-associated DNA-cleaving enzyme Cpf1 also processes precursor CRISPR RNA. *Nature* **2016**, *532*, *517*–*521*.
- (50) Fu, W.; Jiang, L.; van Geest, E. P.; Lima, L. M. C.; Schneider, G. F. Sensing at the Surface of Graphene Field-Effect Transistors. *Adv. Mater.* **2017**, 29, No. 1603610.
- (51) Pachauri, V.; Ingebrandt, S. Biologically sensitive field-effect transistors: from ISFETs to NanoFETs. *Essays Biochem.* **2016**, *60*, 81–90.

- (52) Geim, A. K.; Novoselov, K. S. The rise of graphene. *Nat. Mater.* **2007**, *6*, 183–191.
- (53) Wang, M. C.; Chun, S.; Han, R. S.; Ashraf, A.; Kang, P.; Nam, S. Heterogeneous, three-dimensional texturing of graphene. *Nano Lett.* **2015**, *15*, 1829–1835.
- (54) Lee, C.; Wei, X.; Kysar, J. W.; Hone, J. Measurement of the elastic properties and intrinsic strength of monolayer graphene. *Science* **2008**, *321*, *385*–*388*.
- (55) Seol, J. H.; Jo, I.; Moore, A. L.; Lindsay, L.; Aitken, Z. H.; Pettes, M. T.; Li, X.; Yao, Z.; Huang, R.; Broido, D.; et al. Two-dimensional phonon transport in supported graphene. *Science* **2010**, 328, 213–216.
- (56) Knott, G. J.; Thornton, B. W.; Lobba, M. J.; Liu, J. J.; Al-Shayeb, B.; Watters, K. E.; Doudna, J. A. Broad-spectrum enzymatic inhibition of CRISPR-Cas12a. *Nat. Struct. Mol. Biol.* **2019**, *26*, 315—321.
- (57) Wu, Y.; Lin, Y. M.; Bol, A. A.; Jenkins, K. A.; Xia, F.; Farmer, D. B.; Zhu, Y.; Avouris, P. High-frequency, scaled graphene transistors on diamond-like carbon. *Nature* **2011**, *472*, 74–78.
- (58) Wu, G.; Tang, X.; Meyyappan, M.; Lai, K. W. C. Doping effects of surface functionalization on graphene with aromatic molecule and organic solvents. *Appl. Surf. Sci.* **2017**, *425*, 713–721.
- (59) Hoffmann, M.; Zhao, S.; Pettengill, J.; Luo, Y.; Monday, S. R.; Abbott, J.; Ayers, S. L.; Cinar, H. N.; Muruvanda, T.; Li, C.; et al. Comparative genomic analysis and virulence differences in closely related salmonella enterica serotype heidelberg isolates from humans, retail meats, and animals. *Genome Biol. Evol.* 2014, 6, 1046–1068.
- (60) Desai, A. N.; Anyoha, A.; Madoff, L. C.; Lassmann, B. Changing epidemiology of Listeria monocytogenes outbreaks, sporadic cases, and recalls globally: A review of ProMED reports from 1996 to 2018. *Int. J. Infect. Dis.* **2019**, *84*, 48–53.
- (61) Pennington, H. Escherichia coli O157. Lancet 2010, 376, 1428–1435.
- (62) Saravanan, A.; Kumar, P. S.; Hemavathy, R. V.; Jeevanantham, S.; Kamalesh, R.; Sneha, S.; Yaashikaa, P. R. Methods of detection of food-borne pathogens: a review. *Environ. Chem. Lett.* **2021**, *19*, 189–207.
- (63) Ceuppens, S.; Li, D.; Uyttendaele, M.; Renault, P.; Ross, P.; Ranst, M. V.; Cocolin, L.; Donaghy, J. Molecular Methods in Food Safety Microbiology: Interpretation and Implications of Nucleic Acid Detection. *Compr. Rev. Food Sci. Food Saf.* **2014**, *13*, 551–577.
- (64) Janda, J. M.; Abbott, S. L. 16S rRNA gene sequencing for bacterial identification in the diagnostic laboratory: pluses, perils, and pitfalls. *J. Clin. Microbiol.* **2007**, *45*, 2761–2764.
- (65) Liu, Y.; Cao, Y.; Wang, T.; Dong, Q.; Li, J.; Niu, C. Detection of 12 Common Food-Borne Bacterial Pathogens by TaqMan Real-Time PCR Using a Single Set of Reaction Conditions. *Front. Microbiol.* **2019**, *10*, 222.
- (66) Ramachandran, A.; Santiago, J. G. CRISPR Enzyme Kinetics for Molecular Diagnostics. *Anal. Chem.* **2021**, *93*, 7456–7464.
- (67) Lv, H.; Wang, J.; Zhang, J.; Chen, Y.; Yin, L.; Jin, D.; Gu, D.; Zhao, H.; Xu, Y.; Wang, J. Definition of CRISPR Cas12a Trans-Cleavage Units to Facilitate CRISPR Diagnostics. *Front. Microbiol.* **2021**, *12*, No. 766464.
- (68) Gong, J.; Kan, L.; Zhang, X.; He, Y.; Pan, J.; Zhao, L.; Li, Q.; Liu, M.; Tian, J.; Lin, S.; Lu, Z.; Xue, L.; Wang, C.; Tang, G. An enhanced method for nucleic acid detection with CRISPR-Cas12a using phosphorothioate modified primers and optimized gold-nanopaticle strip. *Bioact. Mater.* **2021**, *6*, 4580–4590.
- (69) Yue, H.; Shu, B.; Tian, T.; Xiong, E.; Huang, M.; Zhu, D.; Sun, J.; Liu, Q.; Wang, S.; Li, Y.; et al. Droplet Cas12a Assay Enables DNA Quantification from Unamplified Samples at the Single-Molecule Level. *Nano Lett.* **2021**, *21*, 4643–4653.
- (70) Cao, Y.; Zheng, Z.; Monbouquette, H. G. Nucleic acid amplification-free detection of DNA and RNA at ultralow concentration. *Curr. Opin. Biotechnol.* **2021**, *71*, 145–150.
- (71) Campos, R.; Borme, J.; Guerreiro, J. R.; Machado, G., Jr.; Cerqueira, M. F.; Petrovykh, D. Y.; Alpuim, P. Attomolar Label-Free

ACS Sensors pubs.acs.org/acssensors Article

Detection of DNA Hybridization with Electrolyte-Gated Graphene Field-Effect Transistors. ACS Sens. 2019, 4, 286–293.

- (72) Broughton, J. P.; Deng, X.; Yu, G.; Fasching, C. L.; Servellita, V.; Singh, J.; Miao, X.; Streithorst, J. A.; Granados, A.; Sotomayor-Gonzalez, A.; et al. CRISPR-Cas12-based detection of SARS-CoV-2. *Nat. Biotechnol.* **2020**, *38*, 870–874.
- (73) Wu, G.; Zhang, N.; Matarasso, A.; Heck, I.; Li, H.; Lu, W.; Phaup, J. G.; Schneider, M. J.; Wu, Y.; Weng, Z.; et al. Implantable Aptamer-Graphene Microtransistors for Real-Time Monitoring of Neurochemical Release in Vivo. *Nano Lett.* **2022**, *22*, 3668–3677.

# **□** Recommended by ACS

CRISPR-Cas-Driven Single Micromotor (Cas-DSM) Enables Direct Detection of Nucleic Acid Biomarkers at the Single-Molecule Level

Desheng Chen, Zhengping Li, et al.

MARCH 21, 2023

ANALYTICAL CHEMISTRY

READ 🗹

Development of a Naked Eye CRISPR-Cas12a and -Cas13a Multiplex Point-of-Care Detection of Genetically Modified Swine

Yuan Wang, Shengsong Xie, et al.

JULY 11, 2023

ACS SYNTHETIC BIOLOGY

READ **C** 

Metal-Organic Framework-DNA Bio-Barcodes Amplified CRISPR/Cas12a Assay for Ultrasensitive Detection of Protein Biomarkers

Wenxiu Long, Yujun Song, et al.

DECEMBER 21, 2022

ANALYTICAL CHEMISTRY

READ 🗹

Harnessing Multiplex crRNA in the CRISPR/Cas12a System Enables an Amplification-Free DNA Diagnostic Platform for ASFV Detection

Muchu Zeng, Xianting Ding, et al.

JULY 20, 2022

ANALYTICAL CHEMISTRY

READ 🗹

Get More Suggestions >